Promotion of Phenol Photodecomposition over TiO_2 Using Au, Pd, and Au–Pd Nanoparticles

Ren Su,[†] Ramchandra Tiruvalam,[§] Qian He,[§] Nikolaos Dimitratos,[‡] Lokesh Kesavan,[‡] Ceri Hammond,[‡] Jose Antonio Lopez-Sanchez,[‡] Ralf Bechstein,[†] Christopher J. Kiely,[§] Graham J. Hutchings,[‡,*] and Flemming Besenbacher[†,*]

[†]Interdisciplinary Nanoscience Center (iNANO) and Department of Physics and Astronomy, Aarhus University, Ny Munkegade, DK-8000 Aarhus C, Denmark, [‡]Cardiff Catalysis Institute, School of Chemistry, Cardiff University, CF10 3AT, Cardiff, U.K., and [§]Department of Materials Science and Engineering, Lehigh University, 5 East Packer Avenue, 18015-3195, Bethlehem, Pennsylvania, USA

ABSTRACT

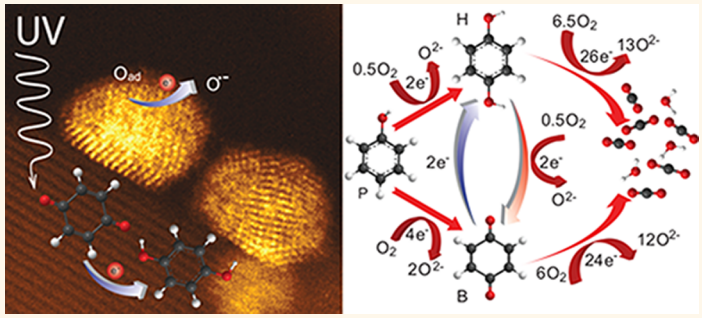

Noble metal nanoparticles (Au, Pd, Au–Pd alloys) with a narrow size distribution supported on nanocrystalline TiO_2 (M/TiO_2) have been synthesized *via* a sol-immobilization route. The effect of metal identity and size on the photocatalytic performance of M/TiO_2 has been systematically investigated using phenol as a probe molecule. A different phenol degradation pathway was observed when using M/TiO_2 catalysts as compared to pristine TiO_2. We propose a mechanism to illustrate how the noble metal nanoparticles enhance the efficiency of phenol decomposition based on photoreduction of *p*-benzoquinone under anaerobic conditions. Our results suggest that the metal nanoparticles not only play a role in capturing photogenerated electrons, but are strongly involved in the photocatalytic reaction mechanism. The analysis of the reaction intermediates allows us to conclude that on M/TiO_2 undesired redox reactions that consume photogenerated radicals are effectively suppressed. The analysis of the final products shows that the reusability performance of the catalyst is largely dependent on the pretreatment of the catalyst and the identity of the metal nanoparticle. Interestingly, the as-prepared Pd and Au–Pd decorated TiO_2 materials exhibit excellent long-term photoactivity, in which ~90% of the phenol can be fully decomposed to CO_2 in each cycle.

KEYWORDS: photocatalysis · TiO_2 · Au · Pd · Au–Pd alloys · phenol decomposition mechanism · reusability · CO_2 conversion

Over the past two decades, titanium dioxide (TiO_2) has been widely applied in heterogeneous (photo) catalysis including hydrogen production,[1,2] water purification,[3,4] and air detoxification,[5,6] owing to its high stability, nontoxicity, and relative abundance.[7] The photocatalytic efficiency of TiO_2, was successfully enhanced by engineering the crystal structure,[8–10] microstructure,[2,11] and impurity concentration.[12,13] Thereby, the recombination kinetics, charge separation efficiency and charge trapping efficiency of TiO_2 can also be controlled.[14,15]

One promising route to enhance the photocatalytic performance of TiO_2 is to decorate the surface with metal nanoparticles (*e.g.*, Ag, Au, Pt, and Pd).[1,14,16–29] It has been shown that the presence of the metal nanoparticles can effectively shift the Fermi level of TiO_2, which results in enhanced photocatalytic reduction efficiency.[1,30]

The application of these metal–semiconductor composite materials to water/air purification has also received great attention. Both model compounds[25–27,30–37] and industrially relevant pollutants[17,22–24,29,36,38,39] have been selected as probe molecules to characterize the efficiency of TiO_2-supported noble metal nanoparticles. Time-resolved experiments have demonstrated that charge-transfer and charge-separation processes at the metal-TiO_2 interface can be tuned by varying the metal identity,[14] the loading of the metal,[16] the ratio of cationic-to-metallic species,[19] and the nanoparticle size.[20] However, some contradictory reports show that metal decoration is not always beneficial, as it can decelerate certain photocatalytic reactions.[30,36] Recently, it has been suggested that the presence of metal nanoparticles might effectively capture photogenerated electrons, which potentially prolongs the lifetime of radicals and may effectively improve the catalytic efficiency.[14,40] Although it appears to be generally accepted that metal nanoparticles mainly trap photogenerated electrons and slow down the recombination of surface radicals, their role in the specific catalytic cycle remains unclear.

* Address correspondence to hutch@cardiff.ac.uk, fbe@inano.au.dk.

Received for review April 19, 2012 and accepted June 4, 2012.

Published online June 04, 2012
10.1021/nn301718v

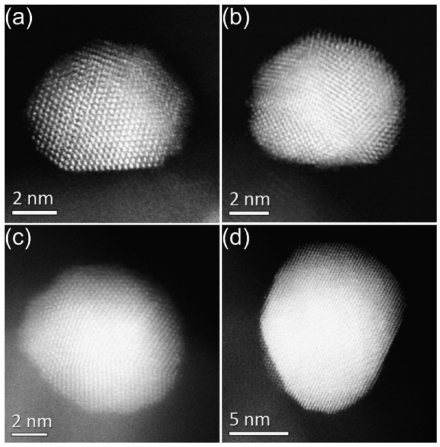

Figure 1. Representative HAADF-STEM images of individual Au particles in (a) Au/TiO_2@120 °C; (b) Au/TiO_2@200 °C; (c) Au/TiO_2@300 °C; and (d) Au/TiO_2@400 °C.

Another important aspect that might limit the application of M/TiO_2 composite catalysts is the reusability of the catalyst material[38,41] and its ability to yield only nontoxic products (*i.e.*, ideally CO_2). Unfortunately, these important parameters are rarely explored in experiments that characterize the performance of M/TiO_2. In fact, leaching from the solid to the liquid phase is a serious issue in the case of supported noble metals in heterogeneous catalysis.[36] Moreover, the metal−semiconductor interface might also undergo chemical changes during long-term irradiation,[38,42] which could potentially result in the production of harmful byproduct. A comprehensive understanding of the photocatalytic performance of M/TiO_2 requires characterization of the reaction mechanism, the efficiency, and the reusability.

In this study, we have investigated the photocatalytic performance of a series of M/TiO_2 (M = Au, Pd, Au−Pd) nanoparticles. Specifically, we supported metal nanoparticles on TiO_2 *via* sol-immobilization and subjected them to a systematic series of heat treatments. We quantified the particle size and investigated the effect of metal identity and annealing procedure on the photocatalytic performance using phenol as a probe reactant molecule. We analyzed the intermediates of the phenol decomposition reaction in air and of the photoreduction of *p*-benzoquinone under anaerobic conditions. Thereby, we explored the reaction mechanism, which allows us to explain differences in efficiency between TiO_2 and M/TiO_2 by the ability of M/TiO_2 to suppress undesired reduction reactions. We have also evaluated the reusability performances, as well as the final products of phenol decomposition. Clearly, the type of metal and the precise details of the calcination treatment have considerable impact on the reusability of M/TiO_2.

RESULTS AND DISCUSSION

Structural Characterization. As-dried sol-immobilized M/TiO_2 (M = Au, Pd, Au−Pd) and calcined Au/TiO_2 catalysts, named as Au/TiO_2@120 °C, Pd/TiO_2@120 °C, Au−Pd/TiO_2@120 °C, and Au/TiO_2@200 °C, Au/TiO_2@300 °C, Au/TiO_2@400 °C, have been investigated in this study. High angle annular dark field (HAADF) imaging in a scanning transmission electron microscope (STEM) was carried out to study the size, structure and morphology of the metal nanoparticles.[43,44] Figure 1 and Supporting Information, Figure S3 show representative HAADF−STEM images of individual Au particles in the Au/TiO_2 samples. The Au/TiO_2 samples show that a mixture of cub-octahedral, decahedral, and icosahedral gold particles persists after immobilization and calcination, with the distribution of the Au particle morphologies being related to the heat-treatment temperature. An increase in the calcination temperature leads to a significant increase in the fraction of gold particles having a cub-octahedral morphology. We also noted that the Au particles tend to progressively form flatter and more extended interfaces with the titania support particles as the calcination temperature was increased.[43]

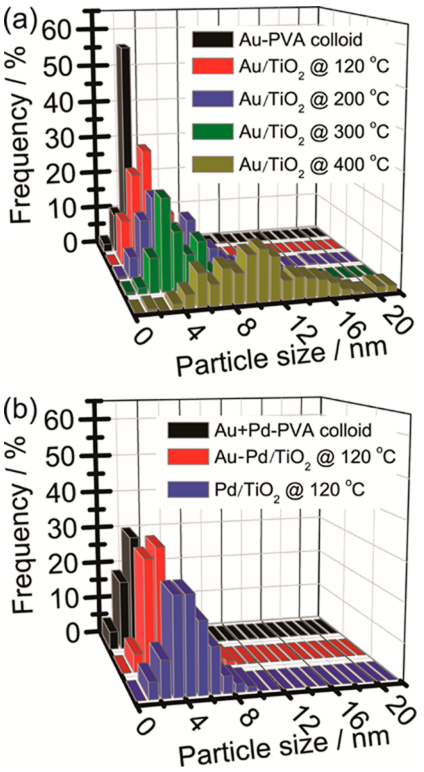

Figure 2. (a) Histograms of the particle size distributions of the as-synthesized Au colloid and the sol-immobilized Au/TiO_2 samples after various calcination treatments; (b) particle size distributions of the as synthesized Au−Pd colloid, and the sol-immobilized and dried Au−Pd/TiO_2 and Pd/TiO_2 samples.

Histograms of the particle size distributions derived from HAADF−STEM images of the Au, Pd, and Au−Pd nanoparticles supported on pristine TiO_2 (Supporting Information, Figure S1) are summarized in Figure 2. The as-synthesized Au and Au+Pd colloids have a mean diameter of 3.0 and 2.9 nm, respectively, and exhibit relatively narrow particle size distributions. A small increase of the mean metal particle size from 3.0 to 3.7 nm for Au/TiO_2, from 2.9 to 3.9 nm for Pd/TiO_2, and from 2.9 to 4.8 nm

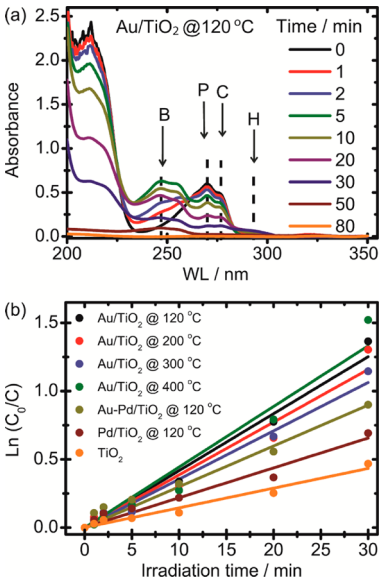

Figure 3. (a) Representative UV−vis absorbance spectra of an aqueous phenol solution after increasing irradiation time using Au/TiO_2 @120 °C as catalyst. The labels B, C, H, and P indicate the absorption peak positions of *p*-benzoquinone, catechol, hydroquinone, and phenol, respectively. (b) Temporal evolution of the total concentration of phenolic compounds. The linear fit to the data represents pseudo-first-order degradation kinetics.

for $Au-Pd/TiO_2$ was observed after the immobilization step (Supporting Information, Figure S2), during which the material is dried in static air at 120 °C for 3 h. On increasing the heat treatment temperature from 120 to 400 °C, we observed a significant growth in the size of the gold nanoparticles at temperatures in excess of 300 °C. In the range of 200 to 300 to 400 °C, the mean particle size increased incrementally from 5.1 to 6.1 to 10.1 nm.

The Effect of Metal Identity and Particle Size on the Photodegradation of Phenol. Phenol was selected as the probe molecule to represent toxic aromatic compounds, which have a low degradability by conventional decomposition methods. Figure 3a representatively shows UV−vis absorbance spectra obtained during phenol photodecomposition using the Au/TiO_2@120 °C catalyst.[45] The phenol content (characterized by the absorbance peak at 275 nm) decreased under irradiation. Meanwhile, the concentration of several intermediates, namely catechol (270 nm), hydroquinone (289 nm), and *p*-benzoquinone (246 nm) are observed to increase. The temporal loss of phenol and evolution of its reaction intermediates was quantitatively analyzed to evaluate the efficiency of the catalyst materials described above. Therefore, we plotted the total concentration of phenolic compounds as a function of irradiation time (Figure 3b) and extracted a decomposition rate assuming pseudo-first-order kinetics.[46] The rate constants are summarized in Table 1. The photocatalytic performance of pristine TiO_2 (P25) was also measured for reference. All M/TiO_2 catalysts exhibit a rate constant that is ~1.5 to 3 times higher than pristine TiO_2. The identity of metal influences

TABLE 1. Comparison of the Photodecomposition Efficiency of Phenol over a Variety of Catalysts Assuming Pseudo-first-order Kinetics

catalyst	mean size (nm)	activity (h^{-1})
Au/TiO_2@120 °C	3.7	2.58 ± 0.12
Au/TiO_2@200 °C	5.1	2.46 ± 0.18
Au/TiO_2@300 °C	6.1	2.22 ± 0.10
Au/TiO_2@400 °C	10.4	2.88 ± 0.21
Pd/TiO_2@120 °C	3.9	1.31 ± 0.07
$Au-Pd/TiO_2$@120 °C	4.8	1.79 ± 0.09
TiO_2	N/A	0.86 ± 0.04

the photoreactivity. It was observed that Pd/TiO_2 and $Au-Pd/TiO_2$ were less active than Au/TiO_2. For Au/TiO_2, the activity is roughly the same regardless of the annealing temperature, that is, mean Au particle size. However, the efficiency is slightly increased after a 400 °C calcination, which might point to an improved contact between the metal and semiconductor nanoparticles established during high-temperature annealing.

The Effect of Metal Nanoparticle Identity and Size on the Mechanism of Phenol Photodegradation. To explore how the metal nanoparticles participate in the catalytic cycle, we followed the evolution of the reaction intermediates during the phenol photodecomposition process, as demonstrated in Figure 4. When pristine TiO_2 was irradiated (Figure 4a), the phenol concentration [P] declined exponentially. Significant accumulation of hydroquinone was observed within the first 30 min of irradiation while benzoquinone and catechol were only found in negligible amounts. The hydroquinone concentration ([H]) reached a maximum of ~100 μM, that is, 25 % of the phenol starting concentration. Only after the concentration ratio of [P]:[H] dropped below unity did [H] begin to decrease. Clearly, the decomposition of hydroquinone dictates the decay of the phenolic compounds over pristine TiO_2. Similar observations have been reported previously,[47−49] implying that the hydroquinone pathway is the rate limiting step for phenol decomposition over pristine TiO_2.

Phenol decomposition over M/TiO_2, however, exhibited a completely different characteristic compared to pristine TiO_2 (Figures 4b−f). All the hydroxylated phenolic intermediates mentioned above were evolved during the irradiation process, but only in small amounts. Typically *p*-benzoquinone and catechol were observed to emerge within the first few minutes and, thereafter, hydroquinone started to evolve. This finding is independent of the identity of the metal and of the metal particle size. The decay of phenol is noticeably faster over M/TiO_2 (Figure 4b−f) than over pristine TiO_2. Note that ~75% of the phenolic compounds were decomposed within 30 min using the Au/TiO_2, whereas only ~35% could be oxidized when using pristine TiO_2.

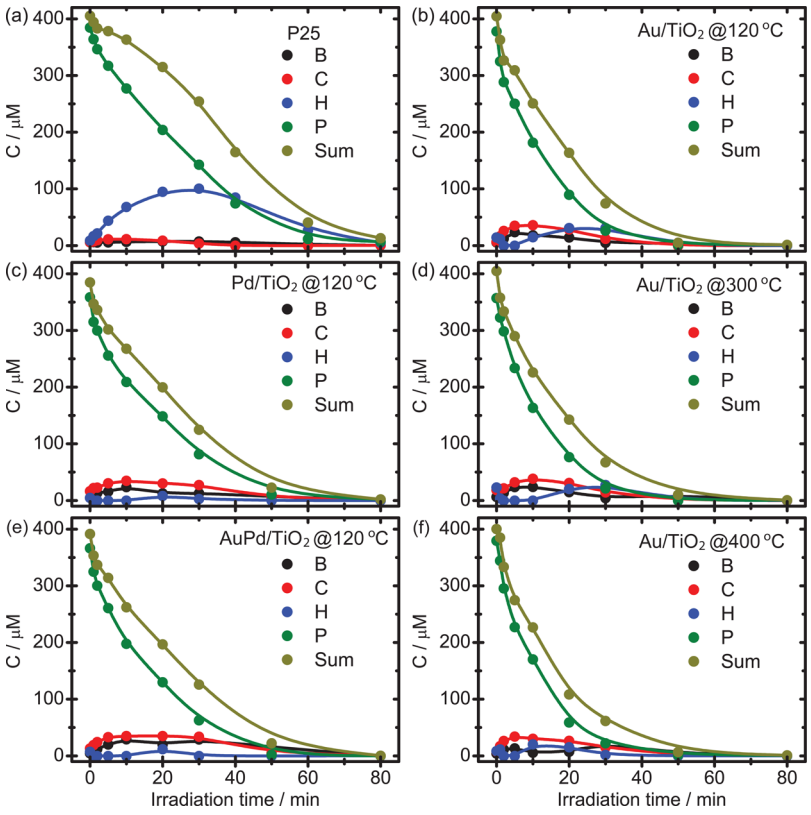

Figure 4. Representative temporal evolution of phenol and the hydroxylated phenolic intermediates derived from UV−vis spectra using (a) pristine TiO_2 (P25), (b) Au/TiO_2@120 °C, (c) Pd/TiO_2@120 °C, (d) Au/TiO_2@200 °C, (e) Au−Pd/TiO_2@120 °C, and (f) Au/TiO_2@400 °C, respectively. [B], [C], [H], and [P] indicate the *p*-benzoquinone, catechol, hydroquinone, and phenol concentration curves, respectively.

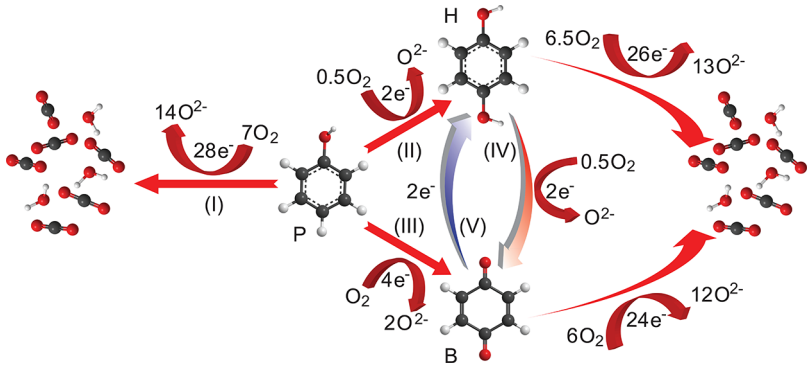

Scheme 1. Proposed photodegradation pathways of phenol. P, H, and B indicate phenol, hydroquinone, and *p*-benzoquinone, respectively.

The photoinduced decomposition of phenol in the presence of titania-based photocatalysts is illustrated by Scheme 1. Phenol can undergo either a direct ring-opening process *via* pathway I or an indirect ring cleavage process *via* pathways II or III, where the hydroxylated phenolic intermediates and its oxidized form, mainly hydroquinone, and *p*-benzoquinone, are generated by the nonselective attack of •OH radicals.[50] All these intermediates can eventually be oxidized to CO_2 *via* various subintermediates following the ring-opening processes.[50−52] Alternatively, photoinduced electron/hole pairs can also participate in the redox reaction (pathways IV and V) described by eqs 1 and 2:

$$\text{benzoquinone} + 2e^- + 2H^+ \xrightarrow{k_{BH}} \text{hydroquinone} + H_2O \quad (1)$$

$$\text{hydroquinone} + 0.5O_2 \xrightarrow{k_{HB}} \text{benzoquinone} + H_2O \quad (2)$$

where k_{BH} and k_{HB} are the rate constants for benzoquinone reduction and hydroquinone oxidation, respectively.

As indicated in Scheme 1, a minimum of seven oxygen molecules is required to fully oxidize a single phenol molecule and 28 electrons are necessary for this oxidation process. The optimum efficiency is only reached

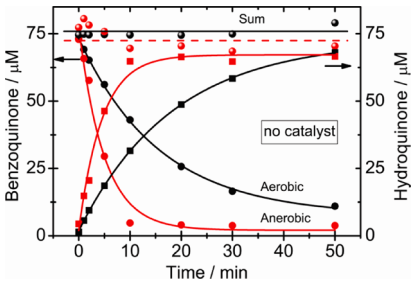

Figure 5. The evolution of benzoquinone, hydroquinone, and their sum during photoinduced benzoquinone reduction in aerobic and anaerobic environments, in the absence of a catalyst. The concentration of dissolved oxygen in the anaerobic environment is ~5 μM as monitored by mass spectrometry.

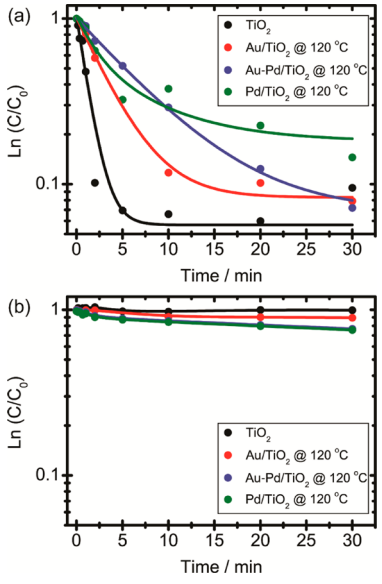

Figure 6. (a) Photoinduced benzoquinone reduction using pristine TiO_2 (black), Au/TiO_2@120 °C (red), Au−Pd/TiO_2@120 °C (blue), and Pd/TiO_2@120 °C (green), respectively, in anaerobic environment; (b) evolution of the sum of benzoquinone and hydroquinone.

TABLE 2. A Comparison of the Photoinduced Benzoquinone Reduction Rate over a Variety of Different Catalysts, Analyzed Using a Pseudo-first-order Kinetics Approximation

catalyst	k_{BH} (min^{-1})
P25	−0.86
Au/TiO_2@120 °C	−0.30
Pd/TiO_2@ 120 °C	−0.30
Au−Pd/TiO_2@120 °C	−0.15

if all the photogenerated electrons participate in the oxidation of phenol and its intermediates. If, however, electrons are consumed by the benzoquinone reduction reaction eq 1, the overall efficiency decreases. Even worse, benzoquinone that has unintentionally been reduced to hydroquinone has to be oxidized again, which consumes two electrons more than required by the direct oxidation of benzoquinone. Thus, with each undesired benzoquinone reduction four electrons are wasted. If the kinetics of

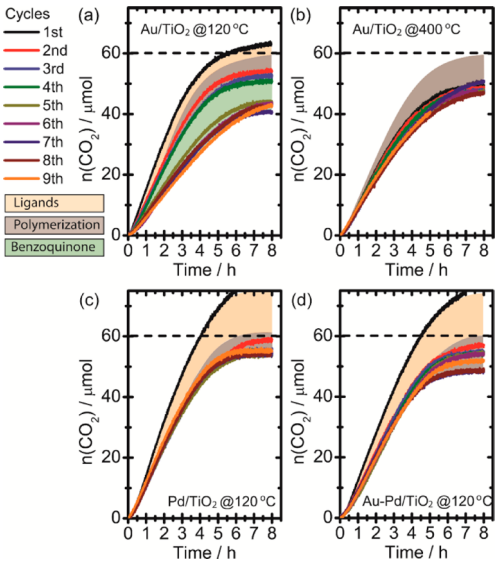

Figure 7. An evaluation of the recycle performance behavior of selected catalyst materials. The final product evolution of phenol degradation using (a) Au/TiO_2@120 °C, (b) Au/TiO_2@400 °C, (c) Pd/TiO_2@120 °C, and (d) Au−Pd/TiO_2@120 °C are shown. The different color-shaded regions indicate (i) the CO_2 originating from breaking the ligands, (ii) the polymerization of phenol, and (iii) the photogeneration of benzoquinone, respectively.

the benzoquinone reduction is faster than, for example, the oxygen reduction process, the consumption of photogenerated radicals by the redox couple B/H will probably dominate. In the worst case, the degradation efficiency will decrease severely and could even vanish. In the case of pristine TiO_2, photo-oxidized benzoquinone produced from phenol or hydroquinone is rapidly reduced to hydroquinone using the photogenerated electrons, which results in the observed accumulation of hydroquinone. This redox reaction rapidly consumes both free electrons and oxygen in an ineffective manner, and consequently inhibits the overall photodecomposition efficiency. Conversely, the accumulation of benzoquinone observed in photodegradation experiments using metal decorated TiO_2 can be associated with the strongly depressed k_{BH}, which suggests that a lot less free electrons and oxygen molecules have been consumed in the redox reactions, thus resulting in an improvement of the overall photooxidation efficiency of phenol.

The alteration of intermediates noted in the phenol decomposition process strongly suggests that the metal nanoparticles actually participate in the catalytic cycle, rather than just playing a more peripheral role in trapping the photogenerated electrons.

To show that metal nanoparticles indeed influence the catalytic reaction in the proposed way, we measured the photoinduced reduction of benzoquinone under anaerobic conditions. For comparison, the reaction was examined in the absence of a catalyst under both aerobic and anaerobic conditions, as shown in Figure 5. It was observed that benzoquinone is reduced to hydroquinone

during irradiation in both cases, but a 3-fold increase in the reduction rate was noted under anaerobic conditions. This can be rationalized from eqs 1 and 2. Whereas benzoquinone reduction is independent of the atmosphere, hydroquinone oxidation requires oxygen. Note that the sum of benzoquinone and hydroquinone remains constant, which suggests that the photolysis of benzoquinone can be neglected.

Similar experiments have been carried out using various photocatalyst materials under anaerobic conditions, as demonstrated in Figure 6 and Table 2. The concentration of dissolved oxygen was kept ~5 μM in all measurements presented in Figure 6.[53] The depletion of benzoquinone was much faster with pristine TiO_2 compared to the photoreduction of benzoquinone in the absence of a catalyst. This finding suggests that benzoquinone reduction is selectively catalyzed on TiO_2 surfaces. Simultaneously, hydroquinone evolves immediately, and the sum of benzoquinone and hydroquinone remains constant (Figure 6b). Interestingly, the benzoquinone reduction rate is strongly depressed when M/TiO_2 is used, regardless of the metal identity. This finding indicates that benzoquinone reduction becomes unfavorable on M/TiO_2 and photogenerated electrons can be more efficiently used, for example, for oxygen reduction.

Assessment of Catalyst Reusability. The reusability performance of selected catalysts for phenol decomposition is depicted in Figure 7. In general, CO_2 evolution started immediately after irradiation commenced, indicating that phenol, and any intermediate products derived from it, are decomposed completely. Note that the final conversion of phenol is compared here rather than the kinetics because CO_2 is soluble in water. A complete turnover of 10 μmol of phenol, the amount that was injected prior to each cycle, would result in the production of 60 μmol of CO_2. However, we do observe some deviations from this ideal situation depending on the specific catalyst used. Figure 7a shows the CO_2 evolution over Au/TiO_2@120 °C. In this case the total amount of CO_2 produced exceeds the expected level in the first cycle, which can be attributed to the photodecomposition of ligands (PVA) still present on the metal.[54] After that the catalyst exhibits a constant turnover in the following three cycles, and ~85% of the phenol is oxidized to CO_2. Meanwhile, insoluble white material started to appear in the liquid. This can be ascribed to a phenol polymerization process.[48] As we could not detect any intermediates of the phenol decomposition process in the liquid phase after 8 h of irradiation, we conclude that the missing 15% of phenol exclusively undergoes polymerization to form the white solid.[55] The Au/TiO_2 catalyst degrades after the fourth cycle, and only 66% of phenol is converted to CO_2. UV–vis spectroscopy (Supporting Information, Figure S6) of the liquid phase confirms that benzoquinone starts to evolve after the fifth cycle.[55] Therefore, ~20% of phenol is partially oxidized to benzoquinone and is not decomposed further during the 8 hour period of UV irradiation. Fascinatingly, the catalyst calcined at 400 °C (Au/TiO_2@400 °C) exhibits an improved reusability, as shown in Figure 7b. Over nine consecutive cycles, 85% of the phenol undergoes full decomposition to CO_2 and the remaining 15% converts into a polymer. Note that there is no CO_2 produced initially from capping agent decomposition in the case of the catalysts that were calcined at higher temperatures, which is in good agreement with the elemental analysis. A STEM-HAADF analysis has been carried out to analyze the Au/TiO_2@400 °C catalyst after its fifth cycle of reusage (Supporting Information, Figure S7).[56] Measurements of the particle size distributions and particle densities were essentially indistinguishable from the unused counterpart. Hence, we conclude that dynamic changes of metal particle size and metal leaching are minimal with successive uses for the high temperature annealed sample. Interestingly, the Pd/TiO_2@120 °C exhibits the best reusability characteristics, as shown in Figure 7c. For this material ~90% of the phenol consistently undergoes full decomposition while the remaining 10% was converted to polymer over all nine cycles. Furthermore, incorporating Au into Pd (i.e., $Au–Pd/TiO_2$@120 °C) *via* alloying does not improve the turnover, but results in a gradual decrease in reusability, as shown in Figure 7d. These reusability test results imply that Au nanoparticles with a larger size might facilitate the polymerization process, whereas the oxidation of benzoquinone is catalyzed better over supported Pd. The incorporation of Au and Pd in the $Au–Pd/TiO_2$ alloy catalyst results in an increase in the polymerization, which again suggests that Pd is less active compared to Au in the polymerization process.

CONCLUSIONS

A series of metal nanoparticles (Au, Pd, Au–Pd alloys) supported on TiO_2 has been synthesized *via* a sol-immobilization method, and their photocatalytic performance has been systematically characterized. Photoinduced phenol oxidation results suggest that TiO_2 decorated with metal nanoparticles are promising candidates for water detoxification applications. We discovered that the metal nanoparticles directly participate in the photocatalytic reactions and play a significant role in suppressing the benzoquinone-to-hydroquinone conversion process. A mechanism has also been proposed in order to explain the superior efficiency of M/TiO_2 materials. Our results suggest that the metal nanoparticles can mediate undesired redox reactions that ineffectively consume photogenerated radicals, thus improving the photo-oxidation efficiency of phenol. It was also found that the temperature employed in the calcination treatment and the identities of the metal strongly influence the reusability

performance of the catalyst. Pd supported on TiO_2 tends to yield a higher conversion to CO_2 and exhibits better long-term photoactivity than the corresponding Au/TiO_2 materials. We are currently exploring the full implications of these findings on other relevant photochemical reactions.

EXPERIMENTAL SECTION

Sample Preparation. A standard sol-immobilization method was utilized to prepare the metal nanoparticles (i.e., Au, Pd, Au−Pd) supported on TiO_2.[57] For the preparation of supported gold and gold−palladium colloids using PVA as a protective ligand, aqueous solutions of $PdCl_2$ and $HAuCl_4 \cdot 3H_2O$ of the desired concentration were prepared. A poly vinyl alcohol (PVA) (1 wt % aqueous solution, Aldrich, MW = 10 000, 80% hydrolyzed) solution was freshly prepared just prior to synthesis of the metal colloid. A representative protocol for preparing a catalyst comprising Au−Pd nanoparticles with 1 wt % total metal loading on a TiO_2 support is as follows. To an aqueous $PdCl_2$ and $HAuCl_4$ solution of the desired concentration, the required amount of a PVA solution (1 wt %) was added (PVA/(Au + Pd) (w/w) = 1.2); a freshly prepared solution of $NaBH_4$ (0.1 M, $NaBH_4$/(Au + Pd) (mol/mol) = 5) was then added to form a dark-brown sol. After 30 min of sol generation, the colloid was immobilized by adding TiO_2 (acidified to pH 1−2 by sulfuric acid) under vigorous stirring conditions. The amount of support material required was calculated to have a total final metal loading of 1 wt %. After 2 h, the slurry was filtered and the catalyst was washed thoroughly with distilled water (neutral mother liquors) and dried at 120 °C overnight. Sol immobilized monometallic gold catalysts were prepared using a similar methodology. Portions of the various dried catalyst materials were calcined at 200, 300, or 400 in static air for 3 h using a heating rate of 5 °C/min.

Structural and Compositional Characterization. *Scanning Transmission Electron Microscopy:*. Samples of sol-immobilized catalysts were prepared for STEM analysis by dry dispersing the catalyst powder onto a holey carbon TEM grid. In the case of the starting Au−PVA and Au + Pd−PVA sols, a drop of the colloidal sol was deposited, and then allowed to evaporate onto a 300-mesh copper TEM grid covered with an ultrathin continuous C film. High-angle annular dark field (HAADF) imaging experiments were carried out using a 200 kV JEOL 2200FS transmission electron microscope equipped with a CEOS aberration corrector.

X-ray Photoelectron Spectroscopy:. X-ray photoelectron spectra were recorded on a Kratos Axis Ultra DLD spectrometer employing a monochromatic Al Kα X-ray source (75−150 W) and analyzer pass energies of 160 eV (for survey scans) or 40 eV (for detailed scans). Samples were mounted using double-sided adhesive tape, and binding energies were referenced to the C(1s) binding energy of adventitious carbon contamination which was taken to be 284.7 eV. In the case of the bimetallic Au−Pd/TiO_2 catalyst, previous studies have shown that the nanoparticles prepared by sol-immobilization are homogeneous Au−Pd alloys[58] with many of the nanoparticles having a multiply twinned morphology.[59] An X-ray photoelectron spectroscopy (XPS) analysis revealed that the colloidal monometallic and bimetallic catalysts dried at 120 °C consisted mainly of metallic Au and Pd.[60]

Elemental Analysis:. Carbon, hydrogen, and nitrogen were analyzed using a CE440 elemental analyzer, whereas chlorine was analyzed using an oxygen flask determination methodology. Inductively coupled plasma−optical emission spectroscopy (ICP-OES) was carried out for the determination of the metal content. Elemental analysis and carbon analysis (Supporting Information, Tables S1 and S2) were performed to examine the chemical composition of the metal supported nanoparticles used in this study.[61] The presence of carbon can be assigned to the polyvinyl alcohol (PVA) ligands used in the synthesis process to encapsulate the metal nanoparticles. A mild calcination at 200 °C removes more than 50% of the carbonaceous species (i.e., the PVA protection layer) and slightly increases the gold nanoparticle size. In contrast, ∼90 wt % of the initial carbonaceous species was removed when the calcinations temperature exceeded 300 °C, and a significant increase in mean particle size to 10.4 nm was observed (Figure 2). Apparently, the destruction of the PVA layer by calcination leads directly to sintering of the particles.

Photocatalytic Reactivity Measurements. Photodecomposition of the phenol solution in ambient condition was performed to evaluate the photocatalytic reactivity of the catalysts. Prior to the measurements, the samples were UV cleaned to remove the capping agents. The catalyst was added at 1 g/L into 50 mL of phenol solution with a concentration of 400 μM. The suspension was kept in the dark for 1 h to reach adsorption/desorption equilibrium. The suspension was then continuously irradiated by a UV light source (365 nm LED diode *3, Optima 365) and 1.5 mL of the suspension was collected at given time intervals. The suspension was further centrifuged and analyzed using an UV−vis spectrometer (UV-1800, Shimadzu, JP).

The photoinduced reaction in a deaerated environment was performed using a homemade leak tight reactor. This reactor was connected to a mass spectrometer (HPR-20, Hiden, UK) *via* a leak valve (F3−701, VSE, AT). The gas phase composition was analyzed using a secondary electron multiplier (SEM) detector. A 0.05 g (1 g/L) mass of the UV cleaned catalyst was added into the glass reactor with 50 mL of 75 μM benzoquinone solution. A 365 nm LED placed on top of a quartz window served as the UV light source. Prior to the catalytic measurements, the reactor was pumped out using a rotary pump. The residual oxygen was monitored by the mass spectrometer for all experiments.[53] A 1.5 mL volume of the suspension was collected at given time intervals and centrifuged for UV−vis spectrometer analysis.

The extinction coefficients of phenol, benzoquinone, catechol, and hydroquinone were measured independently in order to quantify the evolution of intermediate products. Dilute solutions of various concentrations (10∼320 μM) of the above compounds were analyzed by UV−vis spectrometry, and their extinction coefficient at the characteristic wavelength was determined.[46] The concentration of phenolic compounds was then derived by solving the spectrum as shown in the intermediates calculation section in Supporting Information.[46]

Reusability testing of the catalyst was executed using the same leak-tight reactor apparatus. A 0.05 g portion of a 1 g/L as-received catalyst was added into the glass reactor along with 50 mL of phenol solution (200 μM). An 8 h irradiation was applied for each cycle. After each cycle, 2 mL of the irradiated suspension was collected and centrifuged for UV−vis spectrometry analysis. Meanwhile, 2 mL of concentrated (5 mM) phenol solution (that corresponds to 10 μmol phenol) was added into the suspension. The extracted suspension was disposed without recollection of the catalyst; that is to say, ∼4% of the catalyst material was discarded after each cycle. However, there is more than sufficient catalyst material in the suspension at all times to harvest all the light as can be seen, for instance as seen in Figure 7b. The method for calculating of total amount of CO_2 produced is shown in the catalyst reusability section of the Supporting Information.[54]

Conflict of Interest: The authors declare no competing financial interest.

Acknowledgment. The authors gratefully acknowledge financial support from the Center of Energy Materials (CEM) and from iNANO through the Danish Strategic Research Council as well as from the Carlsberg Foundation. In addition we thank the EPSRC and NSF for financial support.

Supporting Information Available: Detailed characterization of the catalysts, the determination of the intermediate products,

as well as the apparatus for photocatalytic performance analysis. This material is available free of charge *via* the Internet at http://pubs.acs.org.

REFERENCES AND NOTES

1. Bamwenda, G. R.; Tsubota, S.; Nakamura, T.; Haruta, M. Photoassisted Hydrogen-Production From a Water−Ethanol Solution—A Comparison of Activities of Au−TiO_2 and Pt−TiO_2. *J. Photochem. Photobiol., A* **1995**, *89*, 177–189.
2. Han, Z.; Xufan, L.; Tongxiang, F.; Frank, E. O.; Jian, D.; Erwin, M. S.; Di, Z.; Qixin, G. Artificial Inorganic Leafs for Efficient Photochemical Hydrogen Production Inspired by Natural Photosynthesis. *Adv. Mater.* **2009**, *22*, 951–956.
3. Bahnemann, W.; Muneer, M.; Haque, M. M. Titanium Dioxide-Mediated Photocatalysed Degradation of Few Selected Organic Pollutants in Aqueous Suspensions. *Catal. Today* **2007**, *124*, 133–148.
4. Hoffmann, M. R.; Martin, S. T.; Choi, W. Y.; Bahnemann, D. W. Environmental Applications of Semiconductor Photocatalysis. *Chem. Rev.* **1995**, *95*, 69–96.
5. Ao, C. H.; Lee, S. C. Indoor Air Purification by Photocatalyst TiO_2 Immobilized on An Activated Carbon Filter Installed in an Air Cleaner. *Chem. Eng. Sci.* **2005**, *60*, 103–109.
6. Cao, Y. Q.; He, T.; Chen, Y. M.; Cao, Y. A. Fabrication of Rutile TiO_2-Sn/Anatase TiO_2-N Heterostructure and Its Application in Visible-Light Photocatalysis. *J. Phys. Chem. C* **2005**, *114*, 3627–3633.
7. Hernandez-Alonso, M. D.; Fresno, F.; Suarez, S.; Coronado, J. M. Development of Alternative Photocatalysts to TiO_2: Challenges and Opportunities. *Energy Environ. Sci.* **2009**, *2*, 1231–1257.
8. Sun, Q. O.; Xu, Y. M. Evaluating Intrinsic Photocatalytic Activities of Anatase and Rutile TiO_2 for Organic Degradation in Water. *J. Phys. Chem. C* **2010**, *114*, 18911–18918.
9. Andersson, M.; Osterlund, L.; Ljungstrom, S.; Palmqvist, A. Preparation of Nanosize Anatase and Rutile TiO_2 by Hydrothermal Treatment of Microemulsions and Their Activity for Photocatalytic Wet Oxidation of Phenol. *J. Phys. Chem. B* **2002**, *106*, 10674–10679.
10. Pan, J.; Liu, G.; Lu, G. M.; Cheng, H. M. On the True Photoreactivity Order of {001}, {010}, and {101} Facets of Anatase TiO_2 Crystals. *Angew. Chem., Int. Ed.* **2011**, *50*, 2133–2137.
11. Kalousek, V.; Tschirch, J.; Bahnemann, D.; Rathousky, J. Mesoporous Layers of TiO_2 as Highly Efficient Photocatalysts for the Purification of Air. *Superlattices Microstruct.* **2008**, *44*, 506–513.
12. Choi, W. Y.; Termin, A.; Hoffmann, M. R. The Role of Metal-Ion Dopants in Quantum-Sized TiO_2—Correlation between Photoreactivity and Charge-Carrier Recombination Dynamics. *J. Phys. Chem.* **1994**, *98*, 13669–13679.
13. Ohno, T.; Akiyoshi, M.; Umebayashi, T.; Asai, K.; Mitsui, T.; Matsumura, M. Preparation of S-doped TiO_2 Photocatalysts and Their Photocatalytic Activities under Visible Light. *Appl. Catal., A* **2004**, *265*, 115–121.
14. Cozzoli, P. D.; Curri, M. L.; Agostiano, A. Efficient Charge Storage in Photoexcited TiO_2 Nanorod-Noble Metal Nanoparticle Composite Systems. *Chem. Commun.* **2005**, 3186–3188.
15. Hurum, D. C.; Agrios, A. G.; Gray, K. A.; Rajh, T.; Thurnauer, M. C. Explaining the Enhanced Photocatalytic Activity of Degussa P25 Mixed-Phase TiO_2 Using EPR. *J. Phys. Chem. B* **2003**, *107*, 4545–4549.
16. Dawson, A.; Kamat, P. V. Semiconductor-Metal Nanocomposites. Photoinduced Fusion and Photocatalysis of Gold-Capped TiO_2 (TiO_2/Gold) Nanoparticles. *J. Phys. Chem. B* **2001**, *105*, 960–966.
17. Arabatzis, I. M.; Stergiopoulos, T.; Andreeva, D.; Kitova, S.; Neophytides, S. G.; Falaras, P. Characterization and Photocatalytic Activity of Au/TiO_2 Thin Films for Azo-Dye Degradation. *J. Catal.* **2003**, *220*, 127–135.
18. Guo, Y. G.; Wan, L. J.; Bai, C. L. Gold/Titania Core/Sheath Nanowires Prepared by Layer-by-Layer Assembly. *J. Phys. Chem. B* **2003**, *107*, 5441–5444.
19. Subramanian, V.; Wolf, E. E.; Kamat, P. V. Influence of Metal/Metal Ion Concentration on the Photocatalytic Activity of TiO_2−Au Composite Nanoparticles. *Langmuir* **2003**, *19*, 469–474.
20. Subramanian, V.; Wolf, E. E.; Kamat, P. V. Catalysis with TiO_2/Gold Nanocomposites. Effect of Metal Particle Size on the Fermi Level Equilibration. *J. Am. Chem. Soc.* **2004**, *126*, 4943–4950.
21. Li, J.; Zeng, H. C. Nanoreactors—Size Tuning, Functionalization, and Reactivation of Au in TiO_2 Nanoreactors. *Angew. Chem., Int. Ed.* **2005**, *44*, 4342–4345.
22. Orlov, A.; Chan, M. S.; Jefferson, D. A.; Zhou, D.; Lynch, R. J.; Lambert, R. M. Photocatalytic Degradation of Water-Soluble Organic Pollutants on TiO_2 Modified with Gold Nanoparticles. *Environ. Technol.* **2006**, *27*, 747–752.
23. Paramasivalm, I.; Macak, J. M.; Schmuki, P. Photocatalytic Activity of TiO_2-Nanotube Layers Loaded with Ag and Au Nanoparticles. *Electrochem. Commun.* **2008**, *10*, 71–75.
24. Yogi, C.; Kojima, K.; Wada, N.; Tokumoto, H.; Takai, T.; Mizoguchi, T.; Tamiaki, H. Photocatalytic Degradation of Methylene Blue by TiO_2 Film and Au Particles−TiO_2 Composite Film. *Thin Solid Films* **2008**, *516*, 5881–5884.
25. Bannat, I.; Wessels, K.; Oekermann, T.; Rathousky, J.; Bahnemann, D.; Wark, M. Improving the Photocatalytic Performance of Mesoporous Titania Films by Modification with Gold Nanostructures. *Chem. Mater.* **2009**, *21*, 1645–1653.
26. Carneiro, J. T.; Yang, C. C.; Moma, J. A.; Moulijn, J. A.; Mul, G. How Gold Deposition Affects Anatase Performance in the Photocatalytic Oxidation of Cyclohexane. *Catal. Lett.* **2009**, *129*, 12–19.
27. Ismail, A. A.; Bahnemann, D. W.; Bannat, I.; Wark, M. Gold Nanoparticles on Mesoporous Interparticle Networks of Titanium Dioxide Nanocrystals for Enhanced Photonic Efficiencies. *J. Phys. Chem. C* **2009**, *113*, 7429–7435.
28. Silva, C. G.; Juarez, R.; Marino, T.; Molinari, R.; Garcia, H. Influence of Excitation Wavelength (UV or Visible Light) on the Photocatalytic Activity of Titania Containing Gold Nanoparticles for the Generation of Hydrogen or Oxygen from Water. *J. Am. Chem. Soc.* **2011**, *133*, 595–602.
29. Mrowetz, M.; Villa, A.; Prati, L.; Selli, E. Effects of Au Nanoparticles on TiO_2 in the Photocatalytic Degradation of An Azo Dye. *Gold Bull.* **2007**, *40*, 154–160.
30. Mogyorosi, K.; Kmetyko, A.; Czirbus, N.; Vereb, G.; Sipos, P.; Dombi, A. Comparison of the Substrate Dependent Performance of Pt-, Au- and Ag-Doped TiO_2 Photocatalysts in H_2-Production and in Decomposition of Various Organics. *React. Kinet. Catal. Lett.* **2009**, *98*, 215–225.
31. Dobosz, A.; Sobczynski, A. Water Detoxification: Photocatalytic Decomposition of Phenol on Au/TiO_2. *Monatsh. Chem.* **2001**, *132*, 1037–1045.
32. Sonawane, R. S.; Dongare, M. K. Sol-gel Synthesis of Au/TiO_2 Thin Films for Photocatalytic Degradation of Phenol in Sunlight. *J. Mol. Catal., A* **2006**, *243*, 68–76.
33. Centeno, M. A.; Hidalgo, M. C.; Dominguez, M. I.; Navio, J. A.; Odriozola, J. A. Titania-Supported Gold Catalysts: Comparison between the Photochemical Phenol Oxidation and Gaseous CO Oxidation Performances. *Catal. Lett.* **2008**, *123*, 198–206.
34. Hidalgo, M. C.; Murcia, J. J.; Navío, J. A.; Colón, G. Photodeposition of Gold on Titanium Dioxide for Photocatalytic Phenol Oxidation. *Appl. Catal., A* **2011**, *397*, 112–120.
35. Maicu, M.; Hidalgo, M. C.; Colon, G.; Navio, J. A. Comparative Study of the Photodeposition of Pt, Au and Pd on Presulphated TiO_2 for the Photocatalytic Decomposition of Phenol. *J. Photochem. Photobiol., A* **2011**, *217*, 275–283.
36. Primo, A.; Corma, A.; Garcia, H. Titania Supported Gold Nanoparticles as Photocatalyst. *Phys. Chem. Chem. Phys.* **2011**, *13*, 886–910.
37. Zielinska-Jurek, A.; Kowalska, E.; Sobczak, J. W.; Lisowski, W.; Ohtani, B.; Zaleska, A. Preparation and Characterization of Monometallic (Au) and Bimetallic (Ag/Au) Modified-Titania Photocatalysts Activated by Visible Light. *Appl. Catal., B* **2011**, *101*, 504–514.
38. Li, G.; Wang, L. K.; Lv, L.; Zhao, X. S. Preparation and Characterization of SiO_2/TiO_2-Pt Core/Shell Nanostructures

and Evaluation of Their Photocatalytic Activity. *J. Nanosci. Nanotechnol.* **2009**, *9*, 177–184.
39. Zang, L.; Macyk, W.; Lange, C.; Maier, W. F.; Antonius, C.; Meissner, D.; Kisch, H. Visible-Light Detoxification and Charge Generation by Transition Metal Chloride Modified Titania. *Chem.—Eur. J.* **2000**, *6*, 379–384.
40. Takai, A.; Kamat, P. V., Capture, Store, and Discharge. Shuttling Photogenerated Electrons across TiO_2-Silver Interface. *ACS Nano 5*, 7369-7376.
41. Zhang, N.; Liu, S.; Fu, X.; Xu, Y.-J. Synthesis of M@TiO_2 (M = Au, Pd, Pt) Core−Shell Nanocomposites with Tunable Photoreactivity. *J. Phys. Chem. C* **2011**, *115*, 9136–9145.
42. Subramanian, V.; Wolf, E.; Kamat, P. V. Semiconductor Metal Composite Nanostructures. To What Extent Do Metal Nanoparticles Improve the Photocatalytic Activity of TiO_2 Films? *J. Phys. Chem. B* **2001**, *105*, 11439–11446.
43. Lopez-Sanchez, J. A.; Dimitratos, N.; Hammond, C.; Brett, G. L.; Kesavan, L.; White, S.; Miedziak, P.; Tiruvalam, R.; Jenkins, R. L.; Carley, A. F.; *et al.* Facile Removal of Stabilizer-Ligands from Supported Gold Nanoparticles. *Nat. Chem. 3*, 551-556.
44. STEM images of M/TiO_2 shown in Figure S1, S2, and S3 can be found in the Supporting Information.
45. UV−vis absorbance spectra of pristine TiO_2 and the rest M/TiO_2 shown in Figure S4 can be found in the Supporting Information.
46. Details of the methodology used for extracting the concentration of phenol and the hydroxylated phenolic compounds from the UV−vis spectra are described in "intermediates calculation" section in the Supporting Information.
47. Nagaveni, K.; Sivalingam, G.; Hegde, M. S.; Madras, G. Photocatalytic Degradation of Organic Compounds over Combustion-Synthesized Nano-TiO_2. *Environ. Sci. Technol.* **2004**, *38*, 1600–1604.
48. Chen, J.; Eberlein, L.; Langford, C. H. Pathways of Phenol and Benzene Photooxidation Using TiO_2 Supported on a Zeolite. *J. Photochem. Photobiol., A* **2002**, *148*, 183–189.
49. Palmisano, L.; Schiavello, M.; Sclafani, A.; Martra, G.; Borello, E.; Coluccia, S. Photocatalytic Oxidation of Phenol on TiO_2 Powders—a Fourier-Transform Infrared Study. *Appl. Catal., B* **1994**, *3*, 117–132.
50. Zazo, J. A.; Casas, J. A.; Mohedano, A. F.; Gilarranz, M. A.; Rodriguez, J. J. Chemical Pathway and Kinetics of Phenol Oxidation by Fenton's Reagent. *Environ. Sci. Technol.* **2005**, *39*, 9295–9302.
51. Mokrini, A.; Ousse, D.; Esplugas, S. Oxidation of Aromatic Compounds with UV Radiation/Ozone/Hydrogen Peroxide. *Water Sci. Technol.* **1997**, *35*, 95–102.
52. Scheck, C. K.; Frimmel, F. H. Degradation of Phenol and Salicylic Acid by Ultraviolet Radiation/Hydrogen Peroxide/Oxygen. *Water Res.* **1995**, *29*, 2346–2352.
53. Gas phase composition of the reactor monitored by mass spectrometry shown in Figure S5 can be found in the Supporting Information.
54. Reusability testing of the catalyst was executed using as-received catalyst without any precleanning procedures to check whether the protective ligands can be oxidized to CO_2.
55. UV−vis spectrum of the phenol solution and mass spectrum of the gas phase composition before and after irradiation were recorded after each cycle, as shown in Figure S6 in the Supporting Information.
56. STEM-HAADF image of the Au/TiO_2@400 °C catalyst after fifth use shown in Figure S7 can be found in the Supporting Information.
57. Dimitratos, N.; Villa, A.; Bianchi, C. L.; Prati, L.; Makkee, M. Gold on Titania: Effect of Preparation Method in the Liquid Phase Oxidation. *Appl. Catal., A* **2006**, *311*, 185–192.
58. Elemental and carbon analysis of M/TiO_2 shown in Tables S1 and S2 can be found in the Supporting Information.
59. Kesavan, L.; Tiruvalam, R.; Ab Rahim, M. H.; bin Saiman, M. I.; Enache, D. I.; Jenkins, R. L.; Dimitratos, N.; Lopez-Sanchez, J. A.; Taylor, S. H.; Knight, D. W.; *et al.* Solvent-Free Oxidation of Primary Carbon-Hydrogen Bonds in Toluene Using Au-Pd Alloy Nanoparticles. *Science* **2011**, *331*, 195–199.
60. Tiruvalam, R. C.; Pritchard, J. C.; Dimitratos, N.; Lopez-Sanchez, J. A.; Edwards, J. K.; Carley, A. F.; Hutchings, G. J.; Kiely, C. J. Aberration Corrected Analytical Electron Microscopy Studies of Sol-Immobilized Au Plus Pd, Au{Pd} and Pd{Au} Catalysts Used for Benzyl Alcohol Oxidation and Hydrogen Peroxide Production. *Faraday Discuss.* **2011**, *152*, 63–86.
61. Dimitratos, N.; Lopez-Sanchez, J. A.; Anthonykutty, J. M.; Brett, G.; Carley, A. F.; Tiruvalam, R. C.; Herzing, A. A.; Kiely, C. J.; Knight, D. W.; Hutchings, G. J. Oxidation of Glycerol Using Gold−Palladium Alloy-Supported Nanocrystals. *Phys. Chem. Chem. Phys.* **2009**, *11*, 4952–4961.